Axon collateral pattern of a sparse locus coeruleus norepinephrine neuron in mouse cerebral cortex.

Running title: Axon Collaterals of the LC-NE Projection to the Cortex

Yu-Ming Wu[1,3], Wei-Chen Hung[1], Yun Chang[1,3], Ming-Yuan Min[1,2,*], Hsiu-Wen Yang[3,4,*].

[1]Department of Life Science, College of Life Science, National Taiwan University, Taipei 10617, Taiwan.
[2]Neurobiology and Cognitive Science Center, National Taiwan University, Taipei 10617, Taiwan.
[3]Department of Biomedical Sciences, Chung-Shan Medical University, Taichung 40201, Taiwan.
[4]Department of Medical Research, Chung-Shan Medical University Hospital, Taichung 40201, Taiwan.

***Correspondence:** mymin@ntu.edu.tw; hwy@csmu.edu.tw

Acknowledgments: We thank the Technology Commons, College of Life Science, National Taiwan University for technical support.

Funding: This work was supported by the National Science and Technology Council, Taiwan [Grant No: 111-2320-B-002 -015 -MY3 (MMY) and 113-2320-B-040-021-MY3 (HWY)].

Authors' contributions: YMW, performed the experiments and collected the data. HCW and YC assisted in data analysis. HWY and MYM designed the experiments and drafted the manuscript.

Data availability statement: All data supporting the results of this study are available from the corresponding authors upon reasonable request.

Declaration of interests: The authors report no competing interests.

Abstract

The locus coeruleus (LC) contains predominantly norepinephrine (NE) neurons with widespread axonal projections throughout the brain and plays a critical role in the control of behavior, particularly arousal. Historically, the LC-NE system was thought to perform this function by releasing NE uniformly throughout most brain regions. However, recent evidence suggests that the cortical projections of the LC are modularly organized, allowing coordination of diverse and sometimes opposing functions, such as fear memory formation and extinction. However, many details remain unclear, and answers require data from axon collaterals of sparse neurons. We modified a viral tracing protocol using a dual recombinase system to trace the axonal collaterals of sparse LC neurons projecting to the cingulate cortex (CgC). Our results show that even a small number of LC neurons still have broad cortical projections, but the pattern is not uniform. There are a few major projections with dense fibers and numerous minor projections with sparse innervation. Notably, the major projections, including the rostrosplenial cortex, dorsal hippocampus, somatosensory cortex, and CgC (the injection site for retrograde viral labeling), are functionally related and may coordinate goal-directed navigation. In conclusion, our results suggest that a single LC neuron projects divergently and non-uniformly to the cortex, with major projections coordinating related cortical areas to regulate specific functions, while minor

projections appear less functionally specific. It's likely that each LC-NE neuron plays a role in maintaining arousal through the minor projections.

Introduction

Located bilaterally in the dorsal pons, the locus coeruleus (LC) is composed of a cluster of relatively large norepinephrine (NE) neurons. With its nearly ubiquitous projection in the central nervous system, the LC serves as the primary NE supply to the brain and spinal cord (Schwarz et al., 2015; Aston-Jones and Waterhouse, 2016). Reflecting this anatomical feature, LC NE neurons play an important role in behavioral control (Aston-Jones and Cohen, 2005; Bouret and Sara, 2005; Sales et al., 2019; Poe et al., 2020; Breton-Provencher et al., 2019). Numerous studies correlating EEG patterns and LC firing activity have firmly established a strong, positive, and monotonic relationship between LC firing rate and arousal levels (McCarley and Hobson, 1975; Aston-Jones and Bloom, 1981), with low LC firing rates associated with sedation or sleep, moderate rates associated with high arousal, and highest rates associated with hyperactivity, attention deficit, and anxiety (Aston-Jones and Bloom, 1981; Aston-Jones and Cohen, 2005; Takahashi et al., 2010). Furthermore, LC-NE neuronal activity has been shown to modulate arousal rather than *vice versa* (Carter et al., 2010; Joshi et al., 2016; Lovett-Barron et al., 2017; Breton-Provencher and Sur, 2019; Hayat et al., 2020). Classically, LC-NE neurons are thought to perform such functional roles through a relatively uniform overall projection of NE fibers to the cortex (Morrison et al., 1978; Biegon and Rainbow, 1983; Audet et al., 1988), allowing uniform NE release to act

simultaneously on neurons and circuits throughout the cortex (Poe et al., 2020). However, such a unified conceptualization has recently been challenged to develop a comprehensive and coherent role for the LC in regulating the physiological and behavioral functions uncovered by recent evidence (Aston-Jones and Cohen, 2005; Bouret and Sara, 2005; Hansen and Manahan-Vaughan, 2015; Uematsu et al., 2017; Hirschberg et al., 2017; Takeuchi et al., 2016; McCall et al., 2017; Sales et al., 2019; Poe et al., 2020).

Using immunohistochemistry (IHC) with antibodies against dopamine beta-hydroxylase (DBH), a synthesizing enzyme of NE and therefore a maker of NE neurons, and quantitative analyses, it has been shown that the distribution of NE innervation across different cortical areas is actually not uniform, but rather regionally specific, with a higher density of DBH immunoreactivity (IR) varicosities in the prefrontal cortex compared to the motor, somatosensory, and piriform cortices (Agster et al. , 2013). More recently, a study using trans-synaptic pseudorabies virus tracing to elucidate the input-output relationship of LC-NE neurons has shown that while LC-NE neurons have diverse projections to multiple cortical regions and receive reciprocal inputs primarily from these same regions, the input-output relationship of LC-NE neurons does not appear to be uniform but shows varying degrees of specificity in

specific LC-NE subcircuits (Schwarz et al., 2015). Furthermore, using retrograde viral tracing of all axonal branches from subsets of LC-NE projection neurons to the medial prefrontal cortex (mPFC) and primary motor cortex (M1), Plummer et al. (2020) reported differences in their patterns of axon collateralization, as well as the difference compared to the entire LC. The different patterns of axon collateralization between LC-NE neurons projecting to different cortical regions are consistent with functional studies showing that the LC-NE system orchestrates the two contrasting learning states, facilitatory and extinctive fear learning, via two different LC-to-cortex modules: the amygdala-projecting module and the independent mPFC-projecting module (Uematsu et al., 2017). Similarly, a spinal-projecting module has been identified to promote analgesia in acute pain, whereas an independent prefrontal cortex-projecting module generates aversion in chronic pain (Hirschberg et al., 2017). Furthermore, M1-projecting and mPFC-projecting LC-NE neurons have been reported to have distinct functional profiles in terms of mRNA expression, membrane properties, and spontaneous synaptic activity (Uematsu et al., 2017; Chandler et al., 2014). In summary, empirical evidence has described the intricate anatomical and functional features of the LC-to-cortex projection, revealing a structured organization into distinct functional modules. Understanding this modular arrangement, hereafter referred to as the LC-to-cortex module (LCCM), will provide insights into how the LC-NE system helps to

regulate multiple functions, ensuring a balanced and adaptive response to diverse situations, and ultimately contributing to the overall behavioral and cognitive flexibility of individuals.

While the functional and morphological studies discussed above generally support that the LC-cortical projection may be organized into functional modules, more detailed information remains elusive. In particular, it remains uncertain whether a given LCCM, such as the LC-mPFC module, is composed of numerous LC-NE neurons, each of which exhibits a similar pattern of axon collaterals as the module as a whole, or whether each individual exhibits very different patterns of axon collaterals. This important question can only be addressed when the number of labeled LC-NE neurons is reduced to the single digit or even single neuron level. The aim of this study is to construct LC-to-mPFC projection patterns at the single-digit or single neuron level using the modified Tracing Axon Collaterals (TrAC) method of Plummer et al. (2020). We focus on the cingulate cortex (CgC) of the mPFC because this cortical area plays a critical role in emotional and cognitive functions (O'Doherty et al., 2002; Ito et al., 2003; Sanfey et al., 2003; Walton et al., 2007; Rolls, 2023), receives the highest density of NE fibers compared to other cortical areas (Agster et al., 2013; Schwarz et al, 2015; Plummer et al., 2020) and its function is largely modulated by the LC-NE system to perform

complicated test behaviors such as go/no-go (Bourate and Sara, 2005) and two-alternative forced-choice (2-AFC; Aston-Jones and Cohen, 2005) tests. We found that even a small number of LC neurons still have broad cortical projections, but the pattern is not uniform, with major projections coordinating related cortical areas to regulate specific functions and minor projections that are less functionally specific and likely contribute to the general maintenance of arousal throughout the brain.

Materials and Methods

Animals and stereotactic surgery for viral vector injection

Mice of both sexes were used in all experiments. They were housed and maintained in a temperature-controlled vivarium under a 12-hour light/dark cycle, with food and water available *ad libitum*. All animal experiments were approved by the Institutional Animal Care and Use Committees of NTU & CSMU, and every effort was made to minimize the number of animals used and their suffering. For stereotaxic surgery, mice aged 4-6 weeks were deeply anesthetized, as indicated by the absence of the hind paw withdrawal reflex, with an intraperitoneal injection of a mixture of zoletil (25 mg/kg) and xylazine hydrochloride (15 mg/kg); additional anesthetic doses were administered as required. Animals were then mounted in a stereotaxic apparatus, a small craniotomy was made over the right CgC, and the dura was reflected. A glass pipette

loaded with AAV1-Syn-ChrisomR-tdT (marker AAV; addgene, Cat. No. 105714) to mark the cortical injection site and retrograde AAV-pEF1a-DIO-FLPo-WPRE-hGHpA (rAAV; addgene, Cat. No. 105714) (ratio: marker AAV to rAAV = 1:2) was then slowly advanced into the right CgC using the coordinates (in mm): 1.0 caudal, 0.5 lateral, and 0.8 dorsal to the bregma. A total volume of 100 nl of AAV at a titer greater than $1x10^{13}$ was slowly infused. One week later, mice were again subjected to the same surgical procedures for stereotactic infusion of 100 nl of AAV8-Ef1a-fDIO-GCaMP6s (addgene, Cat. No. 105714) at a titer greater than $1x10^{13}$ into the bilateral LC using the following coordinates (in mm): -5.4 caudal, ±0.8 lateral, and 3.0 dorsal to the lambda. Both sets of coordinates for the CgC and LC were determined according to the Allen Brain Atlas. The tip of the glass pipette was bevelled to an angle of ~40° with a tip opening of 60-80 µm using a microelectrode beveler (BV-10, Sutter Instrument, Novato CA, USA) and connected to a 2.0 µL Hamilton syringe (Neuros Model 7002 KH, Hamilton, Reno, NV, USA). AAV was delivered manually at a rate of 5 nL/min.

Perfusion, Sections and IHC

Mice were deeply anesthetized with urethane (1.3 g/kg) and perfused via the cardiovascular system with 4% paraformaldehyde (PFA) in 0.1 M phosphate buffer (PB). The brain was dissected and postfixed in the same fixative overnight at 4°C. After

fixation, the brain was blocked into forebrain and brainstem (Fig. 1A). The brainstem was cut into 70 μm thick sections in the coronal plane using a vibratome (Lieca VT1000 S, Germany), and serial sections containing the LC were collected and stained with antibodies against tyrosine hydroxylase (TH), which is a marker for NE neurons due to its role as the rate-limiting enzyme for NE synthesis. The experiment was continued only if TH antibody staining showed that the number of labeled LC-NA neurons in the bilateral LC was less than a single digit and all labeled neurons showed TH-IR. In this case, the entire forebrain was sectioned with a vibratome into 70 μm thick sections in the coronal plane, and every third section of the entire consecutive forebrain sections was stained with IHC and examined (Figure 1A). Of these, those covering the CgC were stained by IHC with primary antibodies against TH and GCaMP6s (GFP) labeled with secondary antibodies conjugated to fluorophores with broad absorption/emission spectra. This fluorescence IHC (FIHC) staining was used to validate the viral infusion site showing tdtomato signal (marker AAV) and to confirm that GFP-IR fibers also showed TH-IR and thus originated from the LC. If any GFP-IR fibers were found that did not show TH-IR, the experiment was terminated. The remaining sections were stained with the primary antibodies against GFP alone, followed by staining with biotinylated secondary antibodies and avidin-biotin complex (ABC; VECTASTAIN® Elite® ABC Universal PLUS Kit); IR products were visualized using 3,3'-

diaminobenzidine (DAB) as chromogen. After IHC, FIHC sections were stained with fluorescent Nissl; sections stained with IHC combined with the ABC (IHC/ABC) method and those not used for IHC were stained with conventional Nissl to facilitate identification of cortical regions.

For FIHC, sections were rinsed briefly with PB followed by phosphate-buffered saline (PBS; 0.9% NaCl in PB). Sections were incubated for 1 hour with a solution consisting of 10% normal goat serum (NGS) and 0.1% bovine serum albumin (BSA) in PBST (0.3% Triton in PBS) to block nonspecific reactions, followed by an additional 1-hour incubation with 0.05% thimerosal and 0.01% sodium azide in PBST for antigen retrieval. Sections were then incubated overnight at 4°C in a primary antibody cocktail including rabbit anti-TH (1:500 dilution; Cat. No. 6A2907, Merck Millipore, Burlington, MA, USA) and chicken anti-GFP (1:1000 dilution; Cat. No. ab13970, Abcam Inc., Cambridge, UK). For sections covering the CgC, the tdtomato (ChrisomR-tdT) signal was detected directly without further antibody staining. Sections were then incubated with a secondary antibody cocktail including goat anti-rabbit IgG conjugated to Alexa-594 (1:500 dilutions; Cat. No. A-11012, Thermo Fisher Scientific, Waltham, MA, USA) and goat anti-chicken IgY conjugated to CF®488A (1:1000 dilution; Cat. No. Biotium#20020, Biotium, Fremont, CA, USA) in PBST for 2 hours. Sections

were washed three times for 10 minutes with PBST between antibody incubations. For IHC/ABC method, sections were treated with 3% H_2O_2 in 0.1 M PB for 20 minutes to quench endogenous peroxidase activity, followed by rinsing in 0.1 M PB and PBST. Sections were then preincubated in 10% NGS in PBST for 1 hour to block nonspecific reactions, followed by an additional 1-hour incubation with 0.05% thimerosal and 0.01% sodium azide for antigen retrieval. Sections were then incubated overnight at 4°C in PBST with the same chicken anti-GFP antibodies for FIHC described above. After washing in PBST, sections were incubated with biotinylated goat anti-chicken IgY secondary antibody (1:200 dilution; Cat. No. BA-9010; VectorLabs, Burlingame, CA, USA) in PBST for 1 hour, followed by washing in PBST and incubation with avidin-biotin-horseradish peroxidase complex (VECTASTAIN® Elite® ABC Universal PLUS Kit; VectorLabs) for 1 hour. After three washes with PBST and 0.1 M PB, sections were immersed in 0.05% DAB solution for 10 minutes, 0.004% H_2O_2 was added, and sections were incubated for an additional 10 minutes.

Data Analysis

After completion of the staining procedures, sections containing CgC were examined and photographed using a Zeiss LSM 780 confocal microscope system (Carl Zeiss); the other sections were examined and photographed using a light microscope

system (Zeiss axio observer Z1 with Zen blue 3.1 software). For each section, images of the entire section were taken. The NE fibers and the outlines and landmarks of the section were traced using ImageJ software. The cortical areas constituting the section were identified by counterstaining using the Nissl method. In addition, QuickNII software was used to assist in the registration of labeled fibers and identified cortical areas on the 3D mouse brain atlas. The lengths of the traced NE fibers were measured and a histogram of NE fiber density across all cortical areas was plotted. NE fiber density in a given area was defined as the ratio of the summed NE fiber length in that area to the total cortical areas.

Results

Strategy for tracing axonal collaterals of sparse LC-NE neurons

While the TrAC method described by Plummer et al. (2020) allows reliable and effective tracing of complete axonal collaterals of LC-NE neurons, the method has a potential weakness due to the labeling of too many (up to hundreds) neurons in a single experiment. This could lead to mutual occlusion of parts of their axonal collaterals among the labeled neurons, resulting in loss of valuable information. The TrAC method primarily uses a mouse strain carrying the dual recombinase-responsive fluorescent tracer (FT) allele crossed with a DBH-Flp mouse strain. As a result, only NE neurons in the offspring express both Flp and the dual recombinase-responsive FT allele. The

second recombinase, cre, is then introduced into a subset of LC-NE neurons projecting to the cortical area of interest by infusing a retrograde canine virus carrying cre into that cortical area. This results in the expression of cre and Flp in all retrogradely labeled LC-NE neurons to activate FT expression; consequently, the entire axon collaterals of all LC-NE neurons projecting to the cortical regions infused with the retrograde virus are exposed by anterograde filling of the expressed FT. Obviously, the amount of labeled LC-NE neurons in this method is highly dependent on the amount of retrograde canine virus infused into the cortex and the infection efficiency of the viral vector. Since a viral vector typically has a transfection rate of less than 100%, to reduce the number of labeled neurons, we used dual AAV infusions while maintaining the specificity of genetic tracing with dual recombinase-dependent expression of FT as described by the TrAC method. Specifically, we use TH-cre mice (strain #: 025614, Jackson Laboratory) in which the TH promoter drives cre (the first recombinase) expression. We labeled a subset of LC-NE neurons projecting to the right CgC by infusing rAAV for cre-dependent expression of Flp (the second recombinase) into the cortical region (Figure 1B). Instead of tracking all retrogradely labeled LC-NE neurons as in the original TrAC method using the dual recombinase-responsive FT mouse line, we were able to track axonal collaterals of a further smaller subset of them by infusing AAV for Flp-dependent expression of GCaMP6s (as FT) into the bilateral LC (Figure 1C). Indeed,

we found that the dual AAV injection strategy allowed us to achieve this goal of labeling sparse LC-NE neurons and exposing their axonal collaterals.

CgC-projecting NE neurons appear to be randomly distributed in the LC

After a series of proof-of-concept experiments, we found that the time interval of 1 week between the infusion of rAAV (together with the marker AAV for the expression of tdtomato to mark the cortical injection site) into the CgC and AAV8 for the Flp-dependent expression of GCaMP6s into the LC, as well as the optimal survival time of 10 weeks after infusion of the AAV8, allowed us to obtain the best results (Figure 1A). Notably, we found no NE fibers in the cortex with a survival time of less than 8 weeks after AAV8 infusion, although neurons with TH-IR were observed in the LC. Accordingly, we next performed 10 experiments using the protocol described above (Figure 1A). Examination of LC sections stained with anti-TH antibody revealed that most of the GCaMP6s (GFP)-positive neurons also exhibited TH-IR in the LC, hereafter referred to as NE neurons, in 5 cases. The other 5 cases failed for unknown reasons because no NE neurons were found in the LC. Of the 5 successful cases, 40 NE neurons were labeled in one case, 5 NE neurons plus one neuron showing no TH-IR were labeled in one case, 5 NE neurons were labeled in two cases, and even better, a single NE neuron was labeled in one case (Figure 2A) in the LC ipsilateral to the cortical injection site. When the location of the 61 NE neurons from the 5 cases was constructed

with registration according to the 4th ventricle using QuickNII software, it appears that these projection neurons to the CgC were randomly distributed rather than clustered at a specific location in the LC (Figure 2B). This observation suggests that NE neurons projecting to the CgC do not have a specific topographical location in the LC, an observation consistent with that of Uematsu et al. (2017). Notably, there were also labeled LC-NE neurons in the contralateral LC; the total number of labeled neurons from the 5 cases is 8 cells, and again they appear to be randomly distributed in the contralateral LC (Figure 2B).

LC-NE neurons projecting to the mPFC show a feature of lateralized projection

We further analyzed forebrain sections covering the CgC from the 3 cases in which only 5 (2 cases) and 1 NE neurons (one case) were identified in the ipsilateral LC; these 3 experiments are designated as Mouse# 513 (5 cells), Mouse# 543 (5 cells), and Mouse# 544 (1 cell). We confirmed that the examined GFP-IR fibers at the infusion site showed TH-IR (Figure 3A, B), hence GFP-IR, hereafter referred to as NE fibers. Interestingly, NE fibers were mostly found in the ipsilateral cortical areas and hippocampus; the fibers are very rare in the contralateral cortical and hippocampal areas (Figure 3C; Supplementary Figures 1-3). This observation suggests that although unilateral CgC infusion of rAAV labeled NE neurons on both sides of the LC, these

labeled LC-NE neurons appear to have a lateralized projection to the cortex and hippocampus. A similar feature of lateralized projection has been reported for LC-NE neurons projecting to the spinal cord (Hirschberg et al. 2017). Accordingly, we focused on a quantitative analysis of the distribution patterns of NE fibers in the right cortex. Interestingly, in contrast to the cortex and hippocampus, the projection to the thalamic nuclei seems to be bilateral (Figure 3C; Supplementary Figures 2-3). Quantitative analysis of NE fiber density and distribution pattern was performed only for the 3 cases (mouse #513, mouse #543, and mouse #544); the remaining 2 cases were not further investigated due to too many labeled cells (40) and the presence of a cell that did not show TH-IR in the ipsilateral LC.

Axon projection from sparse LC-NE neurons to the cortex is divergent but not uniform

Upon completion of axon tracing in all even forebrain sections, the lengths of traced NE fibers were measured, and a histogram of the ratio of total NE fiber length in a cortical region to that of the entire cortex (region-to-total fiber length ratio; RTFLR) was plotted to show the distribution pattern of NE fibers across cortical regions. Interestingly, the results show that the distribution of NE fibers from even a handful of LC-NE neurons is still divergent and spans many cortical regions rather than being restricted to a few specific regions (Supplementary Figures 1-3; Supplementary Table

1). However, the pattern is not uniform; in all three cases, the distribution patterns all contain a few cortical regions with fiber densities higher than or roughly equal to those of the CgC (see asterisk in Figure 4) and many regions with densities much lower than those of the CgC (see #543 in Figure 4). Theoretically, LC-NE neurons were labeled by the rAAV because they have a relatively large number of axonal projections to the CgC. Accordingly, we consider cortical regions with NE fiber densities similar to or even higher than the CgC to be the major cortical projections (MjCPs) of retrogradely labeled LC-NE neurons, while the remaining areas with apparently lower densities are their minor cortical projections (MiCPs). Since such a divergent but nonuniform pattern of cortical projection of sparse LC-NE neurons described above is applicable to all three study cases, we further investigate the functional implication of LC-NE neuron projection to the cortex according to the principle of dividing the axonal trajectory of labeled LC-NE neurons in the cortex into the MjCPs and MiCPs (see red lines in Figures 4 and 5), as described in detail in the following sections.

The major projection targets of sparse LC-NE neurons in the cortex are functionally corelated

Figure 4B shows the NE fiber distribution pattern of mouse #543, the core injection site in this case is at approximately Bregma 0.66 and covers mostly the CgC

of the mPFC and a smaller portion in motor cortex 2 (see asterisk in Figure 3A1 and yellow shadow in Supplementary Figure 2). Five NE neurons are labeled in the ipsilateral LC and none in the contralateral LC (see blue circle in Figure 2B). As can be seen, despite the fact that the total number of labeled neurons is as sparse as 5 cells, the pattern shows the divergent but not uniform cortical projection. In this case, RTFLRs in somatosensory cortex 1 (S1), motor cortex 1 (M1), and motor cortex 2 (M2) are approximately equal to or slightly lower than those in the cortical infusion site (the CgC). Notably, the RTFLRs in these cortical regions (including the CgC) appear to be significantly higher than those in all other regions (as indicated by the red dashed line in Figure 4B), with the exception of the retrosplenial cortex (RSC), the dorsal hippocampal cortex (DHpc). In the RSC and DHpc, the RTFLRs are higher than half of the CC and again apparently higher than in all other areas. Furthermore, it should be emphasized that all DHpc regions, including CA1, CA3, and the dentate gyrus (DG), have approximately the same the RTFLRs; in contrast, no NE fibers were found in the ventral hippocampal cortex (VHpc). Thus, in this case, CgC, S1, M1, M2, RSC and DHpc are considered as MjCPs, while the others are considered as MiCPs. Regarding the functional correlations of labeled LC-NE neurons, or referred to as LC-to-cortex modules (LCCMs), with these MjCPs, we hypothesize that the labeled LC-NE neurons (or LCCMs) may be involved in optimizing goal-directed navigation. We speculate that

the modules may help the S1 to detect and process the salient stimulus in the environment, the CgC, which is involved in cognitive control, attention, emotion regulation, and decision making, to resolve conflicts in tasks involving uncertainty or error correction (O'Doherty et al., 2002; Sanfey et al., 2003; Walton et al., 2007; Joshi et al., 2016; Rolls, 2023), and the M1 and M2 to initiate the adaptive motor responses. Furthermore, since the DHpc is heavily involved in spatial memory and navigation (Strange et al., 2024), and the RSC is involved in spatial orientation, especially when integrating environmental memory with ongoing spatial experience (Vann et al., 2009; Mitchell et al., 2018; Alexander et al., 2023), the additional labelling of these two regions further supports our argument that the tagged LCCMs optimize goal-directed navigation by coordinating sensory, motor, and spatial memory information to guide adaptive behavior and efficient navigation through an environment.

In mouse #544, the core cortical injection site was also predominantly located in the CgC (approximately at Bregma 0.98; see yellow shadow in Supplementary Figure 3), and a single NE neuron was labeled in the ipsilateral LC, while 2 were labeled in the contralateral LC (red circle in Figure 2B). Although fewer NE neurons were labeled compared to mouse #543, the distribution of NE fibers across the cortex is again divergent, but not restricted to a few specific regions. In addition to the CgC, the S1,

RSC, and DHpc, including CA1, CA3, and the DG, are again classified as MjCPs because their RTFLRs are higher than those of the CgC (Figure 5A). As can be seen, these elements of MjCPs are similar to those of mouse #543, except that no motor region is included based on the same criteria, reflecting the fact that fewer NE neurons (or LCCMs) were labeled in mouse #544. The functionally correlated CgC, RSC, and DHpc for spatial cognition are classified as MjCPs in this study case as in mouse #543, further supporting the above conclusion based on the results of mouse #543. Interestingly, in mouse #544, while the RTFLR of the VHpc is significantly lower and is classified as a MiCP, the DHpc has a much higher RTFLR than the injection site (the CgC). As in mouse #543, the remaining cortical regions, including the VHpc, have apparently lower RTFLRs and were again classified as MiCPs.

In mouse #513, the core cortical injection site was also located in the anterior CgC (approximately at Bregma 0.26), with some extension into the M2 cortex (see yellow shadow in Supplementary Figure 1). In this case, 5 NE neurons were labeled in the ipsilateral LC and 3 in the contralateral LC (see yellow circle in Figure 2B). Again, even when the total number of labeled NE neurons is less than a single digit, the distribution of NE fibers across the cortex is still divergent, but not uniform (Figure 5B). The histogram of RTFLR shows that cortical regions with a higher value than in the

CgC include the RSC, DHpc, VHpc, S1 and S2 cortices, M2 cortex, and olfactory piriform cortex (PC). In addition, M1 and extrastriate visual area 2 (V2), although slightly less dense, have RTFLRs approximately equivalent to those of the CgC (as indicated by the red dashed line in Figure 5B). Thus, in the case of this study, these cortical areas are considered to be the MjCPs of labeled LC-NE neurons (or LCCMs) in mouse #513, with the remainder considered to be the MiCPs. Note that the functionally correlated CgC, RSC, and DHpc for spatial cognition are again classified as MjCPs. In addition, reflecting the fact that more LC-NE neurons (or LCCMs) are labeled in this study case, many more cortical regions are also classified as MjCPs compared to the other two cases. However, these additional labeled LCCMPs are located in either sensory (S1, S2, V2, PC) or motor (M1, M2) regions. These features are consistent with the idea of functional correlation deduced from the results of the previous two cases, that the tagged LCCMs labeled may be involved in optimizing goal-directed navigation. This idea is further more supported by averaging the RTFLRs of the 3 study cases (Figure 5C). Interestingly, an exception to the MjCP in mouse #513 is that VHpc is also classified as one of the MjCPs.

Discussion

Technical considerations

The protocol developed in this study to sparsely label LC-NE neurons (with a number less than a single digit) projecting to the cortex is based on the simple fact that viral vectors typically have a transfection rate of less than 100%. Accordingly, we expected that injection of rAAV for cre-dependent expression of Flp into the CgC of TH-cre mice would tag a subset of LC-NE neurons projecting to this cortical region to express the recombinase, and that subsequent injection of a second AAV for Flp-dependent expression of GCaMP6s as FT into the LC would result in expression of GCaMP6s in a further reduced number, but not all, of the rAAV-tagged neurons. Indeed, this strategy resulted in a 30% success rate (3 out of 10 experiments) in achieving the goal of labeling CgC-projecting neurons with a number less than a single digit. In this study, rAAV was injected into the CgC because this region has been reported to play a critical role in emotional and cognitive functions, as well as in the evaluation of the reward or cost of a stimulus (O'Doherty et al., 2002; Ito et al., 2003; Roesch and Olson, 2004; Zerbi et al., 2019). Moreover, the CgC receives the highest density of NA fibers compared to other cortical areas (Agster et al., 2013; Plummer et al., 2020), and its function is largely modulated by the LC-NA system (Ason-Jones and Cohen, 2005; Mueller et al., 2008; Hirschberg et al., 2017; Uematsu et al., 2017; Breton-Provencher and Sur, 2019). In addition, GCaMP6s was used to label NE neurons and their axonal collaterals because it is better transported to the terminals by the axonal transport

system and allows functional imaging of labeled NE fibers for future physiological studies. Similar to the TrAC of Plummer et al. (2020), we also used a dual recombinase system to ensure the specificity of the tracing method, which is further demonstrated by the results showing that GCaMP6s-IR examined in the rAAV infusion site are also TH-IR. In conclusion, our protocol is less costly and more accessible for sparse neuron labeling, as all materials used are either public or commercially available. The results of this protocol immediately provide important information for LC studies. For example, while Schwarz et al. (2015) reported that the output of LC-NE neurons lacks uniformity and shows different specificities in certain LC-NE subcircuits, they also found that the axons of LC-NA neurons branch extensively over numerous cortical regions. Our data suggest that this pattern may result from the sum of the outputs of hundreds of individual LC-NA neurons, which have discrete MjCPs and more uniform MiCPs.

A single LC-NE neuron may coordinate a specific brain function through MjCPs

In this study, the CgC was used as the target for labeling LC-NE neurons. Therefore, it is reasonable to expect that the CgC should receive a relatively large number of NE fibers from the labeled LC neurons, and cortical regions that have approximately the same level of NE fiber innervation, defined in this study as the MjCRs, would be simultaneously excited/inhibited for a specific cognitive function

when the labeled LC-NE neurons are activated. For example, the coordinated specific function could be navigating new or complex environments, as suggested in this study, because the CgC, RSC, and DHpc are constantly the MjCPs of labeled LC-NE neurons in all 3 study cases. Studies in humans and animals have delineated a neural network critical for navigation that includes the RSC, DHpc, and laterodorsal/anterior thalamic nucleus (LD/AN). In rodents, these regions have been reported to have reciprocal connections (Van Groen and Wyss, 1990, 1992, 2003; Jones et al., 2005; Kobayashi and Amaral, 2007), and impairments in these regions have been associated with amnesic syndromes and impaired hippocampal-dependent functions (Vann et al., 2009; Mitchell et al., 2018). Since the LD/AN are also key structures in this network, we also analyzed the RTFLRs in these thalamic nuclei. The results show that the labeled LC-NE neurons generally have divergent and obviously bilateral projections to many thalamic regions in 2 of the 3 study cases (Figure 3C, Supplementary Figures 2-3). Although the RTFLRs of the LD/AN do not meet the criteria as one of the MjCPs (Figure 5A,B), except that of mouse #543 (Figure 4B), considering the very small area of the thalamic nuclei compared to the RSC and DHpc, we believe that the labeled LC-NE neurons could still effectively activate the LD/AN to interact with the RSC and DHpc to help the individual orient in space. Indeed, the average RTFLR (Figure 5C) shows that the AN/LD has the highest RTFLR among MiCPs. It should be noted that since we found very rare NE

fibers in the contralateral cortex, the labeled NE neurons in the LC contralateral to the cortical injection site should have a predominately contralateral projection to the cortex, with the fibers possibly decussating at the level of the thalamus. Similarly, labeled NE neurons in the ipsilateral LC to the cortical injection site should also have a predominately ipsilateral projection to the cortex. In addition to the RSC and DHpc, the CgC is consistently classified as one of the MjCPs in all three study cases because it is the cortical region for rAAV infusion to label L- NE neurons. The RSC is reported to have reciprocal connections via retrosplenial pathways to parts of the anterior CgC (Jones et al., 2005; Vann et al., 2009), providing an indirect route for hippocampal influences on the CgC and *vice versa*. Thus, with the involvement of the CgC, it is reasonable to deduce that the network coordinated by the labeled LC-NE neurons (or LCCMs) may also control the decision-making process, especially when navigating new or complex environments.

Among the three cases studied, mouse #544 has the least number of labeled LC-NE neurons (one in the ipsilateral and two in the contralateral LC) and defined MjCPs. In addition to the network controlling decision-based navigation described above (the CgC, RGS, Hpc, and LD/AN), the S1 is also defined as one of the MjCPs. Therefore, the labeled LC-NE neurons (or LCCMs) could be important for regulating attention to

relevant stimuli during navigation. Indeed, anatomical evidence shows that the RSC plays an important role in relaying highly processed sensory information to the hippocampal formation (Vogt and Miller, 1983; Vann et al., 2009), possibly providing a sensory cue for navigation. Thus, from a functional perspective, the S1 also has a high NE fiber density and is labeled as one of the MjCPs, which is not surprising since the LCCMs might be labeled due to their responsibility for coordinating and modulating navigation using somatosensory inputs as sensory cues. It is not certain whether the RTFLR pattern of mouse #544 is a sum of the 3 labeled LC-NE neurons with a similar RTFLR pattern or a sum of the 3 labeled LC-NE neurons each with a unique RTFLR pattern. However, the result of this study case shows that a single LC-NE neuron can have multiple MjCPs that are functionally correlated, because in this case the number of defined MjCPs is greater than the number of labeled LC-NE neurons.

In mouse #543, 5 LC-NE neurons were labeled in the LC ipsilateral to the cortical injection site. Interestingly, although all labeled neurons are ipsilateral, the pattern of the RTFLR is similar to the other 2 study cases where labeled neurons are on both sides of the LC. Since more LC-NE neurons were labeled, it is not surprising that more MjCPs were defined. Interestingly, the defined MjCPs of mouse #543 include not only all elements (CgC, RSC, DHpc, and S1) of mouse #544, but also the M1 and M2

cortices. In other words, in this case, not only the LCCMs regulating spatial cognition are labeled, but also additional LCCMs regulating sensory processing and motor response. Indeed, the LCCMs are labeled together because they appear to be important not only for coordinating attention to relevant stimuli for navigation, but also for coordinating behavior in tasks that require precise sensory-guided action, such as the 2-AFC test. A simulation study based on experiments correlating single-unit LC recordings in monkeys engaged in the 2-AFC suggests that the LC-NE system may enhance test performance by optimizing the processing of the neural network responsible for discriminating the test-relevant stimulus from environmental distractors and subsequently facilitating the motor network governing the behavioral response (Usher et al., 1999; Aston-Jones and Cohen, 2005). Clearly, such a behavioral test would require the activation of sensory (S1) and motor (M1, M2) networks, as well as cortical areas involved in the recognition of the contingency of goal-related stimuli and their reinforcement (the CgC), and spatial cognition and memory (RSC and DHpc). Therefore, it is reasonable to hypothesize that a small subset of NE neurons (or LCCPMs) with MjCPs of the CgC, RSC, DHpc, S1, M1, and M2 to optimize behavioral tests such as 2-AFC could be labeled by rAAV infusion into the CgC. Of the three study cases, mouse #513 has the most labeled LC-NE neurons with 5 and 3 in the ipsilateral and contralateral LC, respectively; therefore, mouse #513 also has the most defined

MjCPs. However, the RTFLR is again very similar to the other two study cases, except that additional sensory areas are defined, including PC, S2, and V2. Interestingly, VHpc is also defined as an MjCP, which is not the case for mouse #543 and mouse #544. This definition of additional sensory cortical regions as MjCPs is not surprising since, as discussed above, navigation requires sensory cues. Therefore, we propose that the 8 labeled NE neurons together with the defined MjCPs may represent LCCMs that coordinate behavior in more complicated environments or in more complicated tests.

In summary, the results from the 3 cases in this study, all of which used CgC as the target for retrograde labeling of LC-NE neurons, show that a subset of LC-NE neurons appears to regulate a complex interplay of spatial memory, sensory processing, motor control, and cognitive functions. These LC-NE neurons likely facilitate goal-directed navigation and decision-making, helping to integrate sensory, motor, and spatial memory systems for efficient and adaptive behavior in dynamic environments. In addition to identifying a collective of LC-NE neurons (LCCMs) that may play a critical role in orchestrating neural networks for tasks requiring flexible attention, memory-guided actions, and spatial navigation with real-time sensory and motor coordination, the results may also delineate a principal organization of the LC to cortex projection for coordinating the operation of neural networks in complex behaviors.

Namely, the LC contains discrete NE neurons with distinct MjCPs that have functional correlations. Furthermore, even a single LC-NE neuron can have multiple such functionally correlated MjCPs. It should be noted that with such an organization of LC-NE projections to the cortex, the inputs from the cortex and other subcortical structures must be specific, but not uniform, so that different combinations of LCCPMs could be activated to coordinate specific behaviors (see graphical abstract in Figure 6).

All LC-NA neurons contribute to the maintenance of consciousness via MiCPs

However, while Schwarz et al. (2015) reported that the cortical projection of LC-NE neurons is not uniform and shows different specificities in specific LC-NE subcircuits, they also found that the axons of LC-NE neurons branch extensively over numerous cortical regions. Similarly, Plummer et al. (2020) not only demonstrated different patterns of axon collateralization between LC-NE neurons projecting to the mPFC and M1, but also observed widespread projection of these LC-NE neurons to various cortical areas, albeit with lower NE fiber density than those projecting to the mPFC and M1. Interestingly, we have similar observations here, as the defined MiCPs are divergent and uniform, but with lower RTFLR. Given that the RTFLRs are so low, it is unlikely that in our study cases there is a labeled LC-NE neuron which had only MiCPs but not MjCPs and was labeled with rAAV infused into one of its MiCPs. Instead,

the current RTFLR pattern in each study case here is more likely due to the sum of all labeled LC-NE neurons with different MjCPs and MiCPs. Namely, the LC-to-cortex projection is organized into different modules, each containing functionally correlated MjCPs to regulate a specific function and MiCPs to contribute to the regulation of arousal. Through this organization, the LC can regulate specific functions, some of which are even opposite, such as formation *vs*. extinction of fear memory (Uemasu et al., 2017) and pro-nociception *vs*. antinociception (Hirschberg et al., 2017), by releasing NE to functionally related cortical regions; at the same time, all LC-NE neurons contribute to the maintenance of arousal during behavior through the small but uniform divergent projections (MiCPs). In other words, the collective of all MiCPs from all LC-NE neurons can efficiently regulate arousal through the simultaneous and diffuse release of NE to the forebrain.

Previous electron microscopy studies have shown that NE can modulate the function of postsynaptic neurons via both conventional synaptic transmission and volumetric transmission (Vizi et al., 2004; Fuxe et al., 2015). In the trigeminal motor nucleus (Mo5), by analyzing a series of ultrathin serial sections covering an entire varicosity exhibiting TH-IR, it is reported that more than 62% of TH-IR terminals formed synaptic connections with motoneurons, as evidenced by the presence of pre-

/postsynaptic membrane specializations (Min et al., 2007). Other varicosities appeared to function by volume transmission, as determined by the presence of clusters of synaptic vesicles and associated presynaptic membrane specialization, but absence of postsynaptic specialization, releasing NE into the extracellular space to activate extrasynaptic adrenergic receptors. We propose that conventional synaptic transmission, with its high degree of functional specificity (both temporal and spatial), serves as a more efficient mechanism for an LCCM to optimize processing in its functionally interconnected MiCPs for flexible behavior. In contrast, volume transmission, with its more diffuse and long-lasting effect, is better suited for an LCCM to maintain a global operation across its MiCPs, thereby helping to support the necessary cognitive vigilance. However, this argument would seem to require further data demonstrating a difference in the ratio of conventional synaptic to volume transmission between the MjCPs and MiCPs of an LCCM.

Conclusions

In this study, we report data on the trajectory of axonal collaterals in the cortex of a handful of LC-NE neurons genetically engineered to express a FT (GCaMP6s) by infusion of rAAV into the CgC. We found that 1. the location of these CgC-projecting neurons is randomly distributed throughout the LC; 2. a unilateral LC contains NE

neurons projecting to the CgC of both cerebral hemispheres. However, the cortical projection of a single NE neuron is lateralized but not bidirectional. Furthermore, a unilateral LC appears to contain a greater number of ipsilateral projection neurons than the contralateral projection; 3. It is likely that the projection of a single LC neuron to the cortex is divergent but not uniform. The divergent projection consists of a few MjCPs with higher NE fiber density and many MiCPs with lower NE fiber density; 4. The MjCPs appear to be interconnected for a specific function, such as navigation, as identified in this study. Based on these observations, we propose that a single LC-NE neuron could coordinate a specific brain function through the MjCPs; at the same time, all LC-NE neurons contribute to maintaining awareness and arousal during behavior through the more divergent but less specific MiCPs (see graphical summary in Figure 6).

References

1. Agster KL, Mejias-Aponte CA, Clark BD, Waterhouse BD (2013). Evidence for a regional specificity in the density and distribution of noradrenergic varicosities in rat cortex. *J Comp Neurol* **521**, 2195–207.

2. Alexander AS, Place R, Starrett MJ, Chrastil ER, Nitz DA (2023). Rethinking retrosplenial cortex: Perspectives and predictions. *Neuron* **111**, 150-175.

3. Aston-Jones G, Bloom FE (1981). Activity of norepinephrine-containing locus coeruleus neurons in behaving rats anticipates fluctuations in the sleep-waking cycle. *J Neurosci* **1**, 876-86.

4. Aston-Jones G, Cohen JD (2005). An integrative theory of locus coeruleus-norepinephrine function: adaptive gain and optimal performance. *Annu Rev Neurosci* **28**, 403-50.

5. Aston-Jones G, Waterhouse BD (2016). Locus coeruleus: from global projection system to adaptive regulation of behavior. *Brain Res* **1465**, 75-8.

6. Audet MA, Doucet G, Oleskevich S, Descarries L (1988). Quantified regional and laminar distribution of the noradrenaline innervation in the anterior half of the adult rat cerebral cortex. *J Comp Neurol* **274**, 307-18.

7. Biegon A, Rainbow TC (1983). Localization and characterization of [3H]desmethylimipramine binding sites in rat brain by quantitative autoradiography. *J Neurosci* **3**, 1069-76.

8. Bouret S, Sara SJ (2005). Network reset: a simplified overarching theory of locus coeruleus noradrenaline function. *Trends Neurosci* **28**, 574-82.

9. Breton-Provencher V, Sur M (2019). Active control of arousal by a locus coeruleus GABAergic circuit. *Nat Neurosci* **22**, 218-28.

10. Carter ME, Yizhar O, Chikahisa S, Nguyen H, Adamantidis A, Nishino S,

Deisseroth K, de Lecea L (2010). Tuning arousal with optogenetic modulation of locus coeruleus neurons. *Nat Neurosci* **13**, 1526-33.

11. Chandler DJ, Gao WJ, Waterhouse BD (2014). Heterogeneous organization of the locus coeruleus projections to prefrontal and motor cortices. *Proc Natl Acad Sci USA* **111**, 6816-21.

12. Fuxe K, Agnati LF, Marcoli M, Borroto-Escuela DO (2015). Volume transmission in central dopamine and noradrenaline neurons and its astroglial targets. *Neurochem Res* **40**, 2600-14.

13. Hansen N, Manahan-Vaughan D (2015). Hippocampal long-term potentiation that is elicited by perforant path stimulation or that occurs in conjunction with spatial learning is tightly controlled by β-adrenoreceptors and the locus coeruleus. *Hippocampus* **25**, 1285-98.

14. Hayat H, Regev N, Matosevich N, Sales A, Paredes-Rodriguez E, Krom AJ, Bergman L, Li Y, Lavigne M, Kremer EJ, Yizhar O, Pickering AE, Nir Y (2020). Locus coeruleus norepinephrine activity mediates sensory-evoked awakenings from sleep. *Sci Adv* **6**, eaaz4232.

15. Hirschberg S, Li Y, Randall A, Kremer EJ, Pickering AE (2017). Functional dichotomy in spinal- vs prefrontal-projecting locus coeruleus modules splits descending noradrenergic analgesia from ascending aversion and anxiety in rats. *Elife* **6**, e29808.

16. Ito S, Stuphorn V, Brown JW, Schall JD (2003). Performance monitoring by the anterior cingulate cortex during saccade countermanding. *Science* **302**, 120 -22.

17. Jones BF, Groenewegen HJ, Witter MP (2005). Intrinsic connections of the cingulate cortex in the rat suggest the existence of multiple functionally segregated networks. *Neuroscience* **133**, 193–207.

18. Joshi S, Li Y, Kalwani RM, Gold JI (2016). Relationships between pupil diameter and neuronal activity in the locus coeruleus, colliculi, and cingulate cortex. *Neuron* **89**, 221-34.

19. Kobayashi Y, Amaral DG (2007). Macaque monkey retrosplenial cortex: III. Cortical efferents *J Comp Neurol* **502**, 810-33.

20. Lovett-Barron M, Andalman AS, Allen WE, Vesuna S, Kauvar I, Burns VM, Deisseroth K (2017). Ancestral Circuits for the Coordinated Modulation of Brain State. *Cell* **171**, 1411-23.

21. McCall JG, Siuda ER, Bhatti DL, Lawson LA, McElligott ZA, Stuber GD, Bruchas MR (2017). Locus coeruleus to basolateral amygdala noradrenergic projections promote anxiety-like behavior. *Elife* 6, e18247.

22. McCarley RW, Hobson JA (1975) Neuronal excitability modulation over the sleep cycle: a structural and mathematical model. *Science* **189**, 58-60.

23. Min MY, Hsu PC, Lu HW, Lin CJ, Yang HW (2007). Postnatal development of noradrenergic terminals in the rat trigeminal motor nucleus: A light and electron

microscopic immunocytochemical analysis. *Anat Rec* **290**, 96-107.

24. Mitchell AS, Czajkowski R, Zhang N, Jeffery K, Nelson AJD (2018). Retrosplenial cortex and its role in spatial cognition. *Brain Neurosci Adv* **2**, 2398212818757098.
25. Morrison JH, Grzanna R, Molliver ME, Coyle JT (1978). The distribution and orientation of noradrenergic fibers in neocortex of the rat: an immunofluorescence study. *J Comp Neurol* **181**, 17-39.

26. Mueller D, Porter JT, Quirk GJ (2008). Noradrenergic signaling in infralimbic cortex increases cell excitability and strengthens memory for fear extinction. *J Neurosci* **28**, 369-75.

27. O'Doherty JP, Deichmann R, Critchley HD, Dolan RJ (2002). Neural responses during anticipation of a primary taste reward. *Neuron* **33**, 815-26.
28. Poe GR, Foote S, Eschenko O, Johansen JP, Bouret S, Aston-Jones G, Harley CW, Manahan-Vaughan D, Weinshenker D, Valentino R, Berridge C, Chandler DJ, Waterhouse B, Sara SJ (2020). Locus coeruleus: a new look at the blue spot. *Nat Rev Neurosci* 21, 644-59.

29. Plummer NW, Chandler DJ, Powell JM, Scappini EL, Waterhouse BD, Jensen P (2020). An Intersectional Viral-Genetic Method for Fluorescent Tracing of Axon Collaterals Reveals Details of Noradrenergic Locus Coeruleus Structure. *eNeuro* **7**, ENEURO.0010-20.2020.

30. Roesch MR, Olson CR (2004) Neuronal activity related to reward value and

motivation in primate frontal cortex. *Science* **304**, 307-10.

31. Rolls ET (2023). Emotion, motivation, decision-making, the orbitofrontal cortex, anterior cingulate cortex, and the amygdala. *Brain Struct Funct* **228,** 1201-1257.

32. Sales AC, Friston KJ, Jones MW, Pickering AE, Moran RJ (2019). Locus coeruleus tracking of prediction errors optimises cognitive flexibility: an active inference model. *PLoS Comput Biol* **15**, e1006267.

33. Sanfey AG, Rilling JK, Aronson JA, Nystrom LE, Cohen JD (2003). The neural basis of economic decision-making in the Ultimatum Game. *Science* **13**, 1755-8.

34. Schwarz LA, Miyamichi K, Gao XJ, Beier KT, Weissbourd B, DeLoach KE, Ren J, Ibanes S, Malenka RC, Kremer EJ, Luo L (2015). Viral-genetic tracing of the input-output organization of a central noradrenaline circuit. *Nature* **524**, 88-92.

35. Strange BA, Witter MP, Lein ES, Moser EI. Functional organization of the hippocampal longitudinal axis (2014). *Nat Rev Neurosci* **15**, 655-69.

36. Takahashi K, Kayama Y, Lin JS, Sakai K (2010). Locus coeruleus neuronal activity during the sleep-waking cycle in mice. *Neuroscience* **169**, 1115-26.

37. Takeuchi T, Duszkiewicz AJ, Sonneborn A, Spooner PA, Yamasaki M, Watanabe M, Smith CC, Fernández G, Deisseroth K, Greene RW, Morris RG (2016). Locus coeruleus and dopaminergic consolidation of everyday memory. *Nature* **537**, 357-62.

38. Uematsu A, Tan BZ, Ycu EA, Cuevas JS, Koivumaa J, Junyent F, Kremer EJ, Witten IB, Deisseroth K, Johansen JP (2017). Modular organization of the brainstem noradrenaline system coordinates opposing learning states. *Nat Neurosci* **20**, 1602-11.

39. Usher M, Cohen JD, Servan-Schreiber D, Rajkowski J, Aston-Jones G (1999). The role of locus coeruleus in regulation of cognitive performance. *Science* **283**, 549-54.

40. Van Groen T, Wyss J M (1990). Connections of the retrosplenial granular a cortex in the rat. *J Comp Neurol* **300**, 593-606.

41. Van Groen T, Wyss JM (1992). Connections of the retrosplenial dysgranular cortex in the rat. *J Comp Neurol* **315**, 200-16.

42. Van Groen T, Wyss JM (2003). Connections of the retrosplenial granular b cortex in the rat. *J Comp Neurol* **463**, 249–63.

43. Vann SD, Aggleton JP, Maguire EA (2009). What does the retrosplenial cortex do? *Nat Rev Neurosci* **10**, 792-802.

44. Vizi ES, Kiss JP, Lendvai B (2004). Nonsynaptic communication in the central nervous system. *Neurochem Int* **45**, 443–51.

45. Vogt BA, Miller MW (1983) Cortical connections between rat cingulate cortex and visual, motor, and postsubicular cortices. *J Comp Neurol* **216**, 192–210.

46. Walton ME, Croxson PL, Behrens TE, Kennerley SW, Rushworth MF (2007). Adaptive decision making and value in the anterior cingulate cortex. *Neuroimage Suppl 2*, T142-54.

47. Zerbi V, Floriou-Servou A, Markicevic M, Vermeiren Y, Sturman O, Privitera M, von Ziegler L, Ferrari KD, Weber B, De Deyn PP, Wenderoth N, Bohacek J (2019). Rapid Reconfiguration of the Functional Connectome after Chemogenetic Locus Coeruleus Activation. *Neuron 103*, 702-18.

Figures and Legends

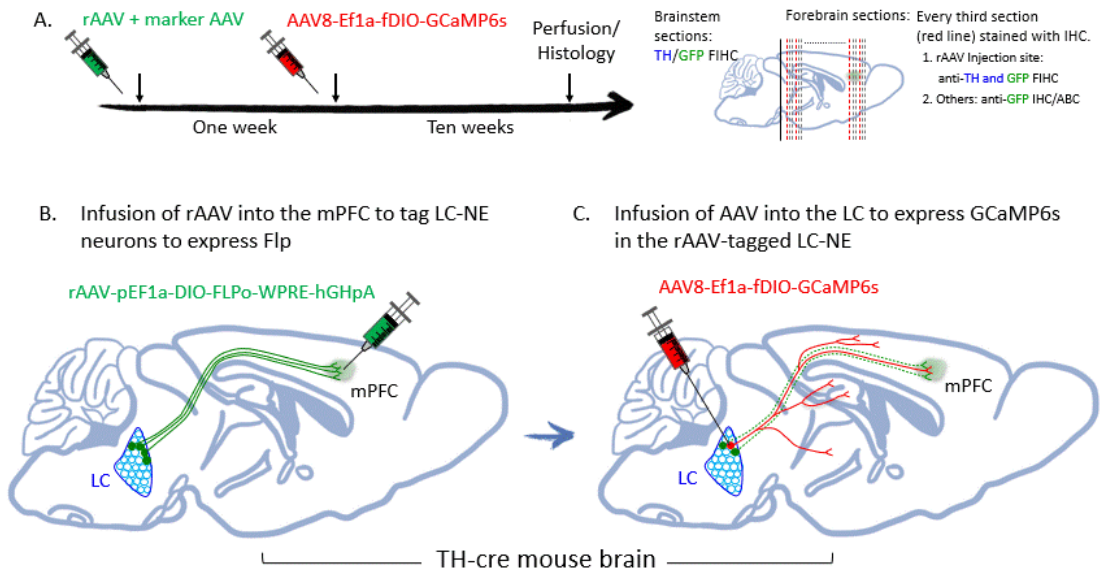

Figure 1. Modified TrAC to reveal whole axon collaterals of sparse LC-NE neurons. ***A***. Timeline of rAAV infusion into the CgC for Cre-dependent expression of Flp, AAV8 infusion into the LC for Flp-dependent expression of GCaMP6s and histological processing (left), and schematic illustrating block (thick line) of brain for brainstem and forebrain sectioning after perfusion and grouping of forebrain sections for IHCs and Nissl staining (right). ***B***. Schematic illustration of retrograde AAV-mediated transduction of a subset of LC-NE neurons projecting to the CgC to express Flp. ***C***. Schematic illustrating the infusion of AAV into the LC to express GCaMP6s in a fraction of rAAV-tagged LC-NE projecting to the CgC.

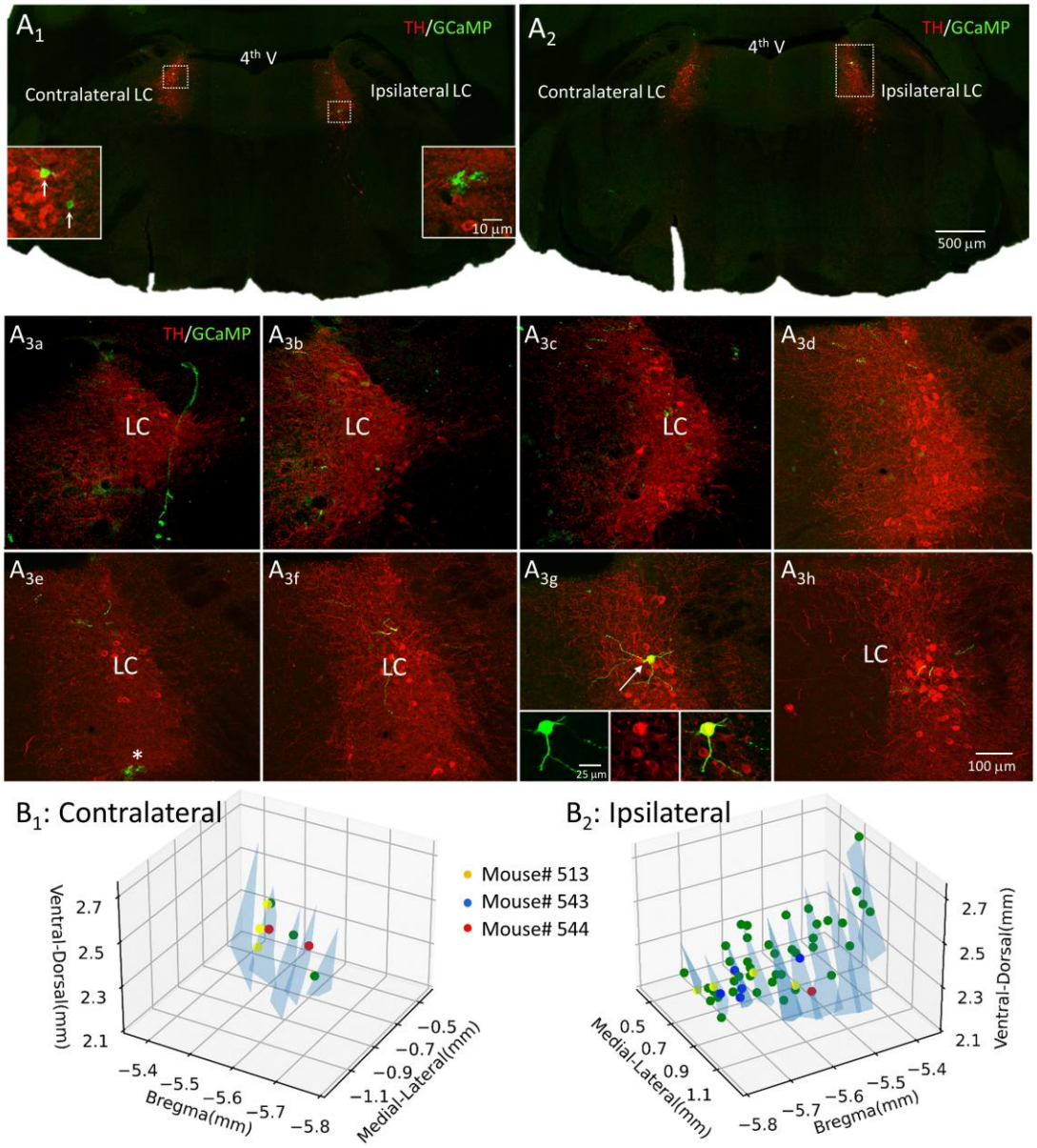

Figure 2. Representative result showing labeling of 3 NE neurons in bilateral LC using the modified TrAC method (data from mouse #544). ***A***. Two low-power images show IHC with primary antibodies against TH (red) and GFP (green). Two and one neurons are labeled in the LC contralateral (A1) and ipsilateral (a2) to the rAAV infusion site, respectively. The lower left inset in A1 is an enlargement of the dotted area of the contralateral LC and shows the two labeled neurons (arrows). Note that the structures in the dashed area of the ipsilateral LC are not neurons, as shown in the lower right inset. Eight high-power images (A3) show sections covering the entire ipsilateral LC; the section (A3g) showing the cell body and proximal dendrites of the labeled neuron is an enlargement of the dashed area shown in A2; also, the insets at the bottom

show the labeled neuron with TH-IR. ***B***. Distribution of all labeled NE (TH- and GFP-IR) neurons in the contralateral (B1) and ipsilateral LC (B2) summarized from the 5 study cases. Yellow, blue, and red circles denote data from mice #513, #543, and #544, respectively; green circle denotes data from the other 2 study cases. The light blue triangular shadow delineates the LC.

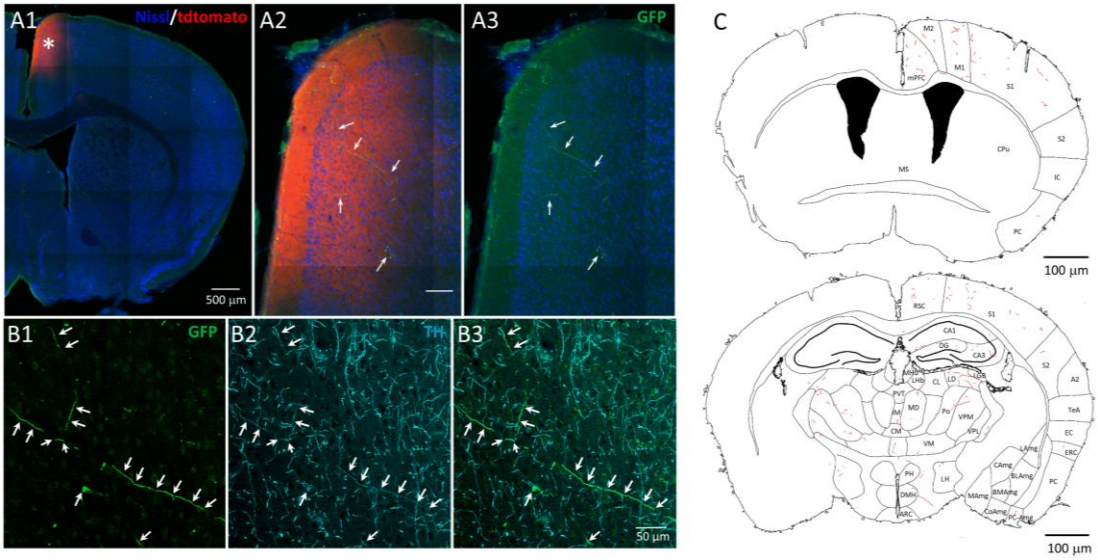

Figure 3. Representative result showing NE (TH and GFP-IR) axons traced in the CgC using the modified TrAC method (data from mouse #543). ***A***. Merged image of tomato (red), GFP (green) and Nissl (blue) staining of one of the forebrain sections covering the viral infusion site (asterisk in A1 marks the CgC). Magnification of the CgC (A2) shows GFP (GCaMP6s)-IR fibers as indicated by arrows. The fibers are better seen when the tdtomato signal is removed (A3). ***B***. Images show the same field from the next consecutive section stained with anti-GFP (GCaMP6s, gray in B1) and anti-TH (cyan in B2) antibodies and the merged image (B3). Note that all GFP (GCaMP6s)-IR fibers also exhibit TH-IR as indicated by the arrows. ***C***. Representative plots of complete tracking of NE fibers in 2 sections stained with IHC/ABC. Note the unilateral and bilateral distribution of NE fibers in the cortex and thalamus (bottom). Brain region abbreviations: **A2**: Secondary auditory cortex; **ARC**: arcuate area (of the hypothalamic area); **BLAmg**: Basolateral amygdala nucleus; **BMAmg**: Basomedial amygdala nucleus; **CA1**: Cornu ammonis area 1 (of the hippocampus); **CA3**: Cornu ammonis area 3 (of the hippocampus); **CAmg**: Central amygdala nucleus; **CL**: Centrolateral thalamic

nucleus; **CM**: Centromedial thalamic nucleus; **CoAmg**: Cortical amygdala nucleus; **CPu**: Caudate putmen (striatum); **DG**: Dentate gyrus (of the hippocampus); **DMH**: Dorsomedial hypothalamic area; **EC**: Ectorhinal cortex; **ERC**: Entorhinal cortex; **IC**: Insular cortex; **IM**: Intermedial thalamic nucleus; **LAmg**: Lateral amygdala nucleus; **LD**: Laterodorsal thalamic nucleus; **LGB**: lateral geniculate body; **LH**: Lateral hypothalamic area; **LHb**: Lateral habenular nucleus; **M1**: Primary motor cortex; **M2**: Secondary motor Cortex; **MAmg**: Medial amygdala nucleus; **MD**: Mediodorsal thalamic nucleus; **MHb**: Medial habenular nucleus; **mPFC**: Medial prefrontal cortex; **MS**: Medial septal nucleus; **PC**: Piliform cortex; **PCAmg**: Piriform-amygdala area; **PH**: Posterior hypothalamic area; **Po**: Posterior thalamic nucleus; **PVT**: Paraventricular thalamic nucleus; **RSC**: Retrosplenial cortex; **S1**: Primary somatosensory cortex; **S2**: Secondary somatosensory cortex; **TeA**: Temporal association cortex; **VM**: Ventromedial thalamic nucleus; **VPL**: Ventral posterolateral thalamic nucleus; **VPM**: Ventral posteromedial thalamic nucleus.

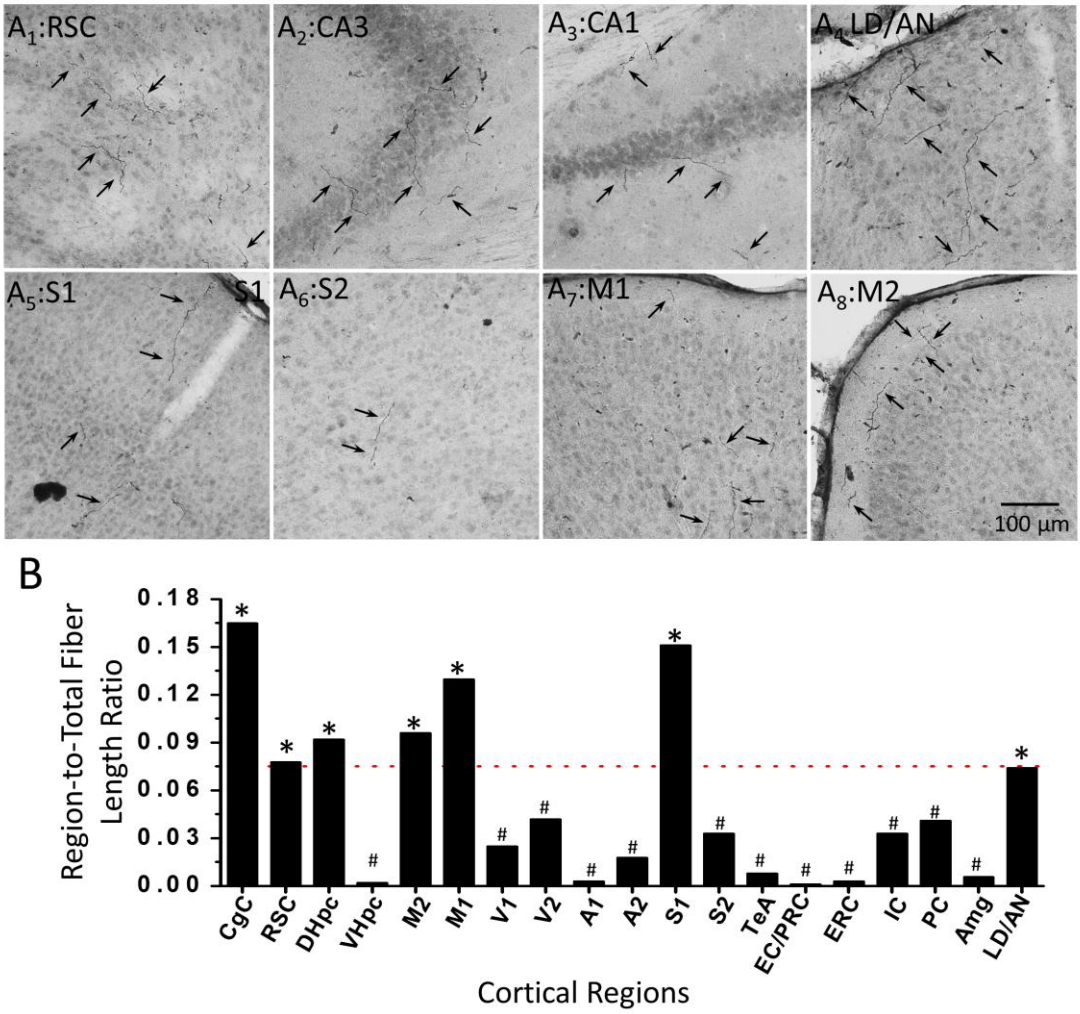

Figure 4. Representative result showing NE axon tracing in other cortical regions using the modified TrAC and anti-GFP IHC-ABC methods (data from mouse #543). ***A***. Representative images of sections not covering the CgC (rAAV infusion site) stained with anti-GFP IHC-ABC showing NE fibers in RSC (A1), CA3 (A2), CA1 (A3), DL/AN (A4), S1 (A5), S2 (A6), M1 (A7), M2 (A8). ***B***. RTFLR histogram of mouse #543. * denotes MjCPs and # denotes MiCPs. The red dotted line shows the separation of MjCPs and MiCPs. Cortical region abbreviations: **A1**: Primary auditory cortex; **A2**: Secondary auditory cortex; **Amg**: Amygdala; **AN**: anterior nucleus (of the thalamus); **CgC**: cingulate cortex; **DHpc**: Dorsal hippocampus; **EC/PRC**: Ectorhinal cortex/ perirhinal cortex; **ERC**, entorhinal cortex; **IC**: Insular cortex; **LD**: laterodorsal nucleus (of the thalamus); **M1**: Primary motor cortex; **M2**: secondary motor cortex; **PC**: Pontine cortex; **RSC**: retrosplenial cortex; **S1**: Primary somatosensory cortex; **S2**: Secondary somatosensory cortex; **TeA**: Temporal association area; **V1**: Primary visual cortex; **V2**: Secondary visual cortex; **VHpc**: Ventral hippocampus.

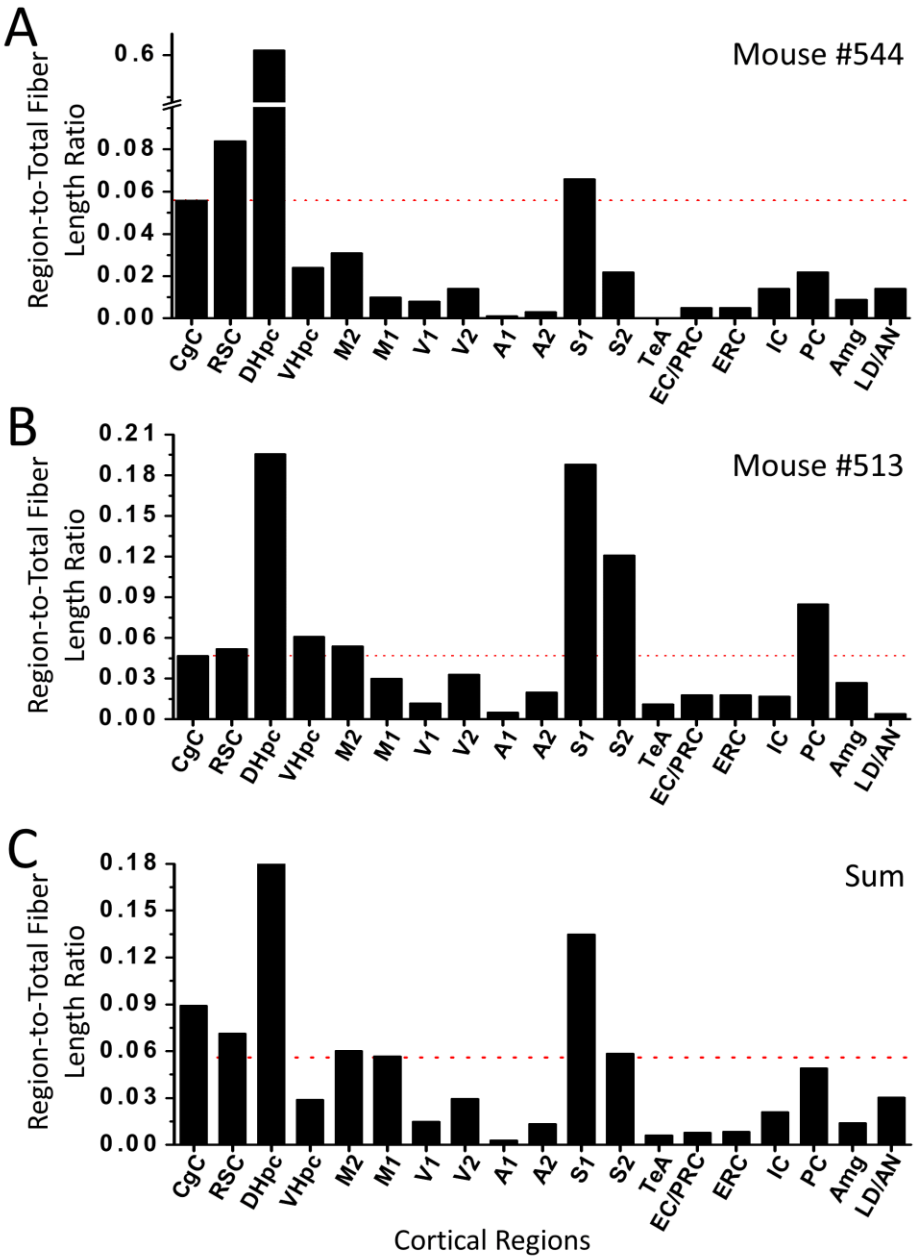

Figure 5. TFLR histograms of mouse #544 (***A***), mouse #513 (***B***) and the sum of the 3 study cases (***C***). The red dotted line shows the separation of MjCPs and MiCPs. See Figure 4 for *abbreviations* of cortical regions.

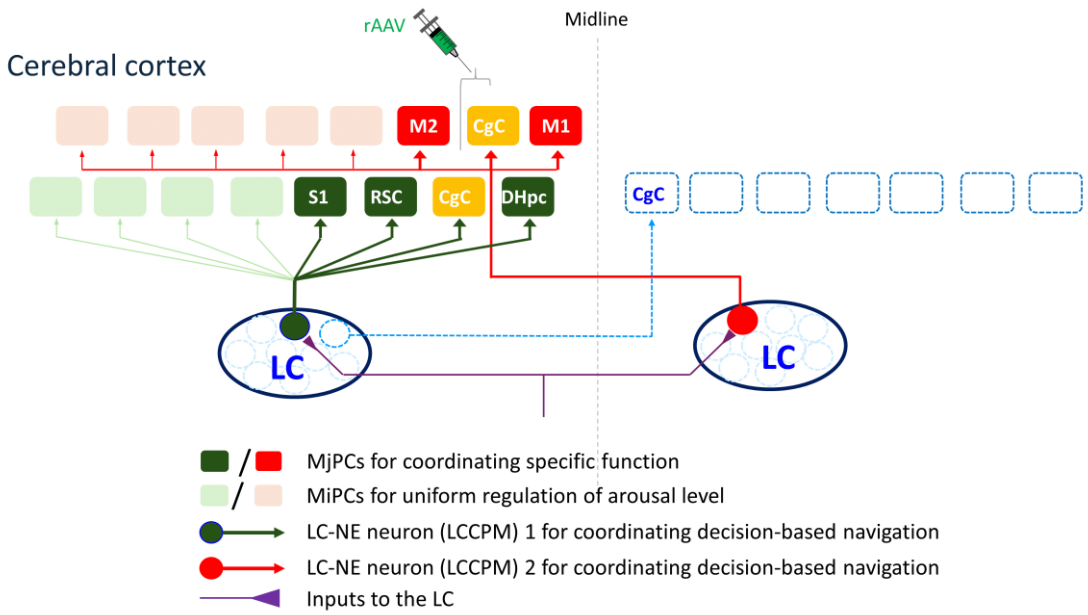

Figure 6. The graphical summary summarizes the conclusions (see the last paragraph of the Discussion).